

Two-particle correlations on transverse momentum and minijet dissipation in Au-Au collisions at $\sqrt{s_{NN}} = 130$ GeV

J. Adams,³ M.M. Aggarwal,²⁹ Z. Ahammed,⁴³ J. Amonett,²⁰ B.D. Anderson,²⁰ D. Arkhipkin,¹³ G.S. Averichev,¹² S.K. Badyal,¹⁹ Y. Bai,²⁷ J. Balewski,¹⁷ O. Barannikova,³² L.S. Barnby,³ J. Baudot,¹⁸ S. Bekele,²⁸ V.V. Belaga,¹² R. Bellwied,⁴⁶ J. Berger,¹⁴ B.I. Bezverkhny,⁴⁸ S. Bharadwaj,³³ A. Bhasin,¹⁹ A.K. Bhati,²⁹ V.S. Bhatia,²⁹ H. Bichsel,⁴⁵ A. Billmeier,⁴⁶ L.C. Bland,⁴ C.O. Blyth,³ B.E. Bonner,³⁴ M. Botje,²⁷ A. Boucham,³⁸ A.V. Brandin,²⁵ A. Bravar,⁴ M. Bystersky,¹¹ R.V. Cadman,¹ X.Z. Cai,³⁷ H. Caines,⁴⁸ M. Calderón de la Barca Sánchez,⁴ J. Carroll,²¹ J. Castillo,²¹ D. Cebra,⁷ Z. Chajecki,⁴⁴ P. Chaloupka,¹¹ S. Chattopdhyay,⁴³ H.F. Chen,³⁶ Y. Chen,⁸ J. Cheng,⁴¹ M. Cherney,¹⁰ A. Chikanian,⁴⁸ W. Christie,⁴ J.P. Coffin,¹⁸ T.M. Cormier,⁴⁶ J.G. Cramer,⁴⁵ H.J. Crawford,⁶ D. Das,⁴³ S. Das,⁴³ M.M. de Moura,³⁵ A.A. Derevschikov,³¹ L. Didenko,⁴ T. Dietel,¹⁴ S.M. Dogra,¹⁹ W.J. Dong,⁸ X. Dong,³⁶ J.E. Draper,⁷ F. Du,⁴⁸ A.K. Dubey,¹⁵ V.B. Dunin,¹² J.C. Dunlop,⁴ M.R. Dutta Mazumdar,⁴³ V. Eckardt,²³ W.R. Edwards,²¹ L.G. Efimov,¹² V. Emelianov,²⁵ J. Engelage,⁶ G. Eppley,³⁴ B. Erazmus,³⁸ M. Estienne,³⁸ P. Fachini,⁴ J. Faivre,¹⁸ R. Fatemi,¹⁷ J. Fedorisin,¹² K. Filimonov,²¹ P. Filip,¹¹ E. Finch,⁴⁸ V. Fine,⁴ Y. Fisyak,⁴ K.J. Foley,⁴ K. Fomenko,¹² J. Fu,⁴¹ C.A. Gagliardi,³⁹ J. Gans,⁴⁸ M.S. Ganti,⁴³ L. Gaudichet,³⁸ F. Geurts,³⁴ V. Ghazikhanian,⁸ P. Ghosh,⁴³ J.E. Gonzalez,⁸ O. Grachov,⁴⁶ O. Grebenyuk,²⁷ D. Grosnick,⁴² S.M. Guertin,⁸ Y. Guo,⁴⁶ A. Gupta,¹⁹ T.D. Gutierrez,⁷ T.J. Hallman,⁴ A. Hamed,⁴⁶ D. Hardtke,²¹ J.W. Harris,⁴⁸ M. Heinz,² T.W. Henry,³⁹ S. Hepplemann,³⁰ B. Hippolyte,⁴⁸ A. Hirsch,³² E. Hjort,²¹ G.W. Hoffmann,⁴⁰ H.Z. Huang,⁸ S.L. Huang,³⁶ E.W. Hughes,⁵ T.J. Humanic,²⁸ G. Igo,⁸ A. Ishihara,⁴⁰ P. Jacobs,²¹ W.W. Jacobs,¹⁷ M. Janik,⁴⁴ H. Jiang,⁸ P.G. Jones,³ E.G. Judd,⁶ S. Kabana,² K. Kang,⁴¹ M. Kaplan,⁹ D. Keane,²⁰ V.Yu. Khodyrev,³¹ J. Kiryluk,²² A. Kisiel,⁴⁴ E.M. Kislov,¹² J. Klay,²¹ S.R. Klein,²¹ A. Klyachko,¹⁷ D.D. Koetke,⁴² T. Kollegger,¹⁴ M. Kopytine,²⁰ L. Kotchenda,²⁵ M. Kramer,²⁶ P. Kravtsov,²⁵ V.I. Kravtsov,³¹ K. Krueger,¹ C. Kuhn,¹⁸ A.I. Kulikov,¹² A. Kumar,²⁹ C.L. Kunz,⁹ R.Kh. Kutuev,¹³ A.A. Kuznetsov,¹² M.A.C. Lamont,⁴⁸ J.M. Landgraf,⁴ S. Lange,¹⁴ F. Laue,⁴ J. Lauret,⁴ A. Lebedev,⁴ R. Lednický,¹² S. Lehocká,¹² M.J. LeVine,⁴ C. Li,³⁶ Q. Li,⁴⁶ Y. Li,⁴¹ S.J. Lindenbaum,²⁶ M.A. Lisa,²⁸ F. Liu,⁴⁷ L. Liu,⁴⁷ Q.J. Liu,⁴⁵ Z. Liu,⁴⁷ T. Ljubicic,⁴ W.J. Llope,³⁴ H. Long,⁸ R.S. Longacre,⁴ M. Lopez-Noriega,²⁸ W.A. Love,⁴ Y. Lu,⁴⁷ T. Ludlam,⁴ D. Lynn,⁴ G.L. Ma,³⁷ J.G. Ma,⁸ Y.G. Ma,³⁷ D. Magestro,²⁸ S. Mahajan,¹⁹ D.P. Mahapatra,¹⁵ R. Majka,⁴⁸ L.K. Mangotra,¹⁹ R. Manweiler,⁴² S. Margetis,²⁰ C. Markert,⁴⁸ L. Martin,³⁸ J.N. Marx,²¹ H.S. Matis,²¹ Yu.A. Matulenko,³¹ C.J. McClain,¹ T.S. McShane,¹⁰ F. Meissner,²¹ Yu. Melnick,³¹ A. Meschanin,³¹ M.L. Miller,²² Z. Milosevich,⁹ N.G. Minaev,³¹ C. Mironov,²⁰ A. Mischke,²⁷ D.K. Mishra,¹⁵ J. Mitchell,³⁴ B. Mohanty,⁴³ L. Molnar,³² C.F. Moore,⁴⁰ D.A. Morozov,³¹ M.G. Munhoz,³⁵ B.K. Nandi,⁴³ S.K. Nayak,¹⁹ T.K. Nayak,⁴³ J.M. Nelson,³ P.K. Netrakanti,⁴³ V.A. Nikitin,¹³ L.V. Nogach,³¹ S.B. Nurushev,³¹ G. Odyniec,²¹ A. Ogawa,⁴ V. Okorokov,²⁵ M. Oldenburg,²¹ D. Olson,²¹ S.K. Pal,⁴³ Y. Panebratsev,¹² S.Y. Panitkin,⁴ A.I. Pavlinov,⁴⁶ T. Pawlak,⁴⁴ T. Peitzmann,²⁷ V. Perevozchikov,⁴ C. Perkins,⁶ W. Peryt,⁴⁴ V.A. Petrov,¹³ S.C. Phatak,¹⁵ R. Picha,⁷ M. Planinic,⁴⁹ J. Pluta,⁴⁴ N. Porile,³² J. Porter,⁴⁵ A.M. Poskanzer,²¹ M. Potekhin,⁴ E. Potrebenikova,¹² B.V.K.S. Potukuchi,¹⁹ D. Prindle,⁴⁵ C. Pruneau,⁴⁶ J. Putschke,²³ G. Rai,²¹ G. Rakness,³⁰ R. Raniwala,³³ S. Raniwala,³³ O. Ravel,³⁸ R.L. Ray,⁴⁰ S.V. Razin,¹² D. Reichhold,³² J.G. Reid,⁴⁵ G. Renault,³⁸ F. Retiere,²¹ A. Ridiger,²⁵ H.G. Ritter,²¹ J.B. Roberts,³⁴ O.V. Rogachevskiy,¹² J.L. Romero,⁷ A. Rose,⁴⁶ C. Roy,³⁸ L. Ruan,³⁶ R. Sahoo,¹⁵ I. Sakrejda,²¹ S. Salur,⁴⁸ J. Sandweiss,⁴⁸ I. Savin,¹³ P.S. Sazhin,¹² J. Schambach,⁴⁰ R.P. Scharenberg,³² N. Schmitz,²³ L.S. Schroeder,²¹ K. Schweda,²¹ J. Seger,¹⁰ P. Seyboth,²³ E. Shahaliev,¹² M. Shao,³⁶ W. Shao,⁵ M. Sharma,²⁹ W.Q. Shen,³⁷ K.E. Shestermanov,³¹ S.S. Shimanskiy,¹² E. Sichtermann,²¹ F. Simon,²³ R.N. Singaraju,⁴³ G. Skoro,¹² N. Smirnov,⁴⁸ R. Snellings,²⁷ G. Sood,⁴² P. Sorensen,²¹ J. Sowinski,¹⁷ J. Speltz,¹⁸ H.M. Spinka,¹ B. Srivastava,³² A. Stadnik,¹² T.D.S. Stanislaus,⁴² R. Stock,¹⁴ A. Stolpovsky,⁴⁶ M. Strikhanov,²⁵ B. Stringfellow,³² A.A.P. Suaide,³⁵ E. Sugarbaker,²⁸ C. Suire,⁴ M. Sumbera,¹¹ B. Surrow,²² T.J.M. Symons,²¹ A. Szanto de Toledo,³⁵ P. Szarwas,⁴⁴ A. Tai,⁸ J. Takahashi,³⁵ A.H. Tang,²⁷ T. Tarnowsky,³² D. Thein,⁸ J.H. Thomas,²¹ S. Timoshenko,²⁵ M. Tokarev,¹² T.A. Trainor,⁴⁵ S. Trentalange,⁸ R.E. Tribble,³⁹ O.D. Tsai,⁸ J. Ulery,³² T. Ullrich,⁴ D.G. Underwood,¹ A. Urkinbaev,¹² G. Van Buren,⁴ M. van Leeuwen,²¹ A.M. Vander Molen,²⁴ R. Varma,¹⁶ I.M. Vasilevski,¹³ A.N. Vasiliev,³¹ R. Vernet,¹⁸ S.E. Vigdor,¹⁷ V.P. Viyogi,⁴³ S. Vokal,¹² S.A. Voloshin,⁴⁶ M. Vznuzdaev,²⁵ W.T. Waggoner,¹⁰ F. Wang,³² G. Wang,²⁰ G. Wang,⁵ X.L. Wang,³⁶ Y. Wang,⁴⁰ Y. Wang,⁴¹ Z.M. Wang,³⁶ H. Ward,⁴⁰ J.W. Watson,²⁰ J.C. Webb,¹⁷ R. Wells,²⁸ G.D. Westfall,²⁴ A. Wetzler,²¹ C. Whitten Jr.,⁸ H. Wieman,²¹ S.W. Wissink,¹⁷ R. Witt,² J. Wood,⁸ J. Wu,³⁶ N. Xu,²¹ Z. Xu,⁴ Z.Z. Xu,³⁶ E. Yamamoto,²¹ P. Yepes,³⁴ V.I. Yurevich,¹² Y.V. Zanevsky,¹² H. Zhang,⁴ W.M. Zhang,²⁰ Z.P. Zhang,³⁶ P.A. Zolnierczuk,¹⁷ R. Zoukarneev,¹³ Y. Zoukarneeva,¹³ and A.N. Zubarev¹²

(STAR Collaboration)

¹*Argonne National Laboratory, Argonne, Illinois 60439*
²*University of Bern, 3012 Bern, Switzerland*
³*University of Birmingham, Birmingham, United Kingdom*
⁴*Brookhaven National Laboratory, Upton, New York 11973*
⁵*California Institute of Technology, Pasadena, California 91125*
⁶*University of California, Berkeley, California 94720*
⁷*University of California, Davis, California 95616*
⁸*University of California, Los Angeles, California 90095*
⁹*Carnegie Mellon University, Pittsburgh, Pennsylvania 15213*
¹⁰*Creighton University, Omaha, Nebraska 68178*
¹¹*Nuclear Physics Institute AS CR, 250 68 Řež/Prague, Czech Republic*
¹²*Laboratory for High Energy (JINR), Dubna, Russia*
¹³*Particle Physics Laboratory (JINR), Dubna, Russia*
¹⁴*University of Frankfurt, Frankfurt, Germany*
¹⁵*Institute of Physics, Bhubaneswar 751005, India*
¹⁶*Indian Institute of Technology, Mumbai, India*
¹⁷*Indiana University, Bloomington, Indiana 47408*
¹⁸*Institut de Recherches Subatomiques, Strasbourg, France*
¹⁹*University of Jammu, Jammu 180001, India*
²⁰*Kent State University, Kent, Ohio 44242*
²¹*Lawrence Berkeley National Laboratory, Berkeley, California 94720*
²²*Massachusetts Institute of Technology, Cambridge, MA 02139-4307*
²³*Max-Planck-Institut für Physik, Munich, Germany*
²⁴*Michigan State University, East Lansing, Michigan 48824*
²⁵*Moscow Engineering Physics Institute, Moscow Russia*
²⁶*City College of New York, New York City, New York 10031*
²⁷*NIKHEF, Amsterdam, The Netherlands*
²⁸*Ohio State University, Columbus, Ohio 43210*
²⁹*Panjab University, Chandigarh 160014, India*
³⁰*Pennsylvania State University, University Park, Pennsylvania 16802*
³¹*Institute of High Energy Physics, Protvino, Russia*
³²*Purdue University, West Lafayette, Indiana 47907*
³³*University of Rajasthan, Jaipur 302004, India*
³⁴*Rice University, Houston, Texas 77251*
³⁵*Universidade de São Paulo, São Paulo, Brazil*
³⁶*University of Science & Technology of China, Anhui 230027, China*
³⁷*Shanghai Institute of Applied Physics, Shanghai 201800, China*
³⁸*SUBATECH, Nantes, France*
³⁹*Texas A&M University, College Station, Texas 77843*
⁴⁰*University of Texas, Austin, Texas 78712*
⁴¹*Tsinghua University, Beijing 100084, China*
⁴²*Valparaiso University, Valparaiso, Indiana 46383*
⁴³*Variable Energy Cyclotron Centre, Kolkata 700064, India*
⁴⁴*Warsaw University of Technology, Warsaw, Poland*
⁴⁵*University of Washington, Seattle, Washington 98195*
⁴⁶*Wayne State University, Detroit, Michigan 48201*
⁴⁷*Institute of Particle Physics, CCNU (HZNU), Wuhan 430079, China*
⁴⁸*Yale University, New Haven, Connecticut 06520*
⁴⁹*University of Zagreb, Zagreb, HR-10002, Croatia*

(Dated: October 20, 2019)

We present the first measurements of two-particle correlations on transverse momentum p_t for Au-Au collisions at $\sqrt{s_{NN}} = 130$ GeV. Significant large-momentum-scale correlation structures are observed for charged primary hadrons with $0.15 \leq p_t \leq 2$ GeV/c and pseudorapidity $|\eta| \leq 1.3$. Such correlations were not observed in a similar study at lower energy and are not predicted by theoretical collision models. The observed correlation structure is consistent with a scenario in which initial-state semi-hard parton scattering and fragmentation are modified by in-medium dissipation.

PACS numbers: 24.60.Ky, 25.75.Gz

Two-particle correlations and associated nonstatistical fluctuations in relativistic heavy ion collisions probe the

dynamics of parton scattering and nonperturbative aspects of quantum chromodynamics [1, 2, 3]. Substan-

tial nonstatistical fluctuations in the event-wise mean transverse momentum $\langle p_t \rangle$ of charged particles from Au-Au collisions have been reported by the STAR [4] and PHENIX [5] experiments at the Relativistic Heavy Ion Collider (RHIC). $\langle p_t \rangle$ fluctuations at RHIC are much larger than those reported at the CERN Super Proton Synchrotron (SPS) with one-tenth the CM energy [6], and were not predicted by theoretical models [4, 7, 8]. Such fluctuations could result from incompletely equilibrated initial-state multiple scattering (ISS) [9] or minijet production [7], the increased hard-scattering cross section at RHIC energies producing greater two-particle correlations there. In this Letter we report the first study of two-particle correlations *on* transverse momentum p_t to probe the dynamical origins of $\langle p_t \rangle$ fluctuations in Au-Au collisions at $\sqrt{s_{NN}} = 130$ GeV (CM energy per nucleon-nucleon pair) observed with the STAR detector at RHIC.

Nonstatistical event-wise $\langle p_t \rangle$ fluctuations, measured as a variance excess by quantity $\Delta\sigma_{p_t:n}^{2(CI)}$ introduced in [4], can be expressed as a p_t -weighted integral of two-particle correlations measured by a pair-ratio distribution. $\Delta\sigma_{p_t:n}^{2(CI)}$ can be rewritten in terms of discrete sums over p_t products [10], in turn approximated by a weighted integral of the difference between pair-number densities for correlated (same-event, sibling) pairs $\rho_{sib}(p_{t1}, p_{t2})$ and uncorrelated (mixed-event) pairs $\rho_{mix}(p_{t1}, p_{t2})$, as

$$\begin{aligned} \Delta\sigma_{p_t:n}^{2(CI)} &\equiv \frac{1}{\varepsilon} \sum_{j=1}^{\varepsilon} \left\{ \frac{1}{n_j} \sum_{i \neq i'=1}^{n_j} (p_{tji} p_{tji'} - \hat{p}_t^2) \right\} \quad (1) \\ &= \frac{1}{\bar{N}} \iint dp_{t1} dp_{t2} p_{t1} p_{t2} (\rho_{sib} - \rho_{mix}) \\ &= (\bar{N} - 1) \hat{p}_t^2 \langle r(p_{t1}, p_{t2}) - 1 \rangle, \end{aligned}$$

where pair ratio $r \equiv \rho_{sib}/\rho_{mix}$ is introduced in the last line. Superscript CI (charge independent) indicates that the sums include all charges, ε is the number of events in a centrality bin, j is the event index, n_j is the number of accepted particles in event j , \hat{p}_t is the mean of the inclusive p_t distribution (all accepted particles from all events in a centrality bin), i and i' are particle indices and \bar{N} is the mean event multiplicity in the acceptance. The angle brackets denote a normalized expectation value with weight $p_{t1} p_{t2} \rho_{mix}(p_{t1}, p_{t2})$. In this paper we present two-particle p_t correlations measured by pair-ratio distribution $r(p_{t1}, p_{t2})$ corresponding to excess $\langle p_t \rangle$ fluctuations.

Data were obtained with the STAR Time Projection Chamber (TPC) [11]. Triggering, tracking details, quality cuts and primary-particle definition are discussed in [4]. Data consisted of 300k events divided into four centrality classes [12] defined by cuts on TPC track multiplicity N within $|\eta| \leq 1.3$, $0.15 \leq p_t \leq 2$ GeV/c, and full azimuthal acceptance. Densities ρ_{sib} and ρ_{mix} were approximated by symmetrized pair-number histograms $n_{kl,sib}$ and $n_{kl,mix}$. Particle pairs were summed into two-dimensional bins (kl) on (p_{t1}, p_{t2}) . Density ratios r were approximated by normalized ratio histograms $\hat{r}_{kl} \equiv \hat{n}_{kl,sib}/\hat{n}_{kl,mix}$, with $\hat{n}_{kl} = n_{kl}/\sum_{kl} n_{kl}$. Correc-

tions were made to \hat{r} for two-track inefficiencies caused by overlapping space points in the TPC and intersecting trajectories reconstructed as > 2 particles [13]. Mixed pairs were formed from event pairs with multiplicities differing by ≤ 100 ($N \sim 10^3$ for central collisions) and primary-vertex axial positions differing by ≤ 7.5 cm [14].

The centrality dependence of differential quantity $\hat{r} - 1$ is shown in Fig. 1 for four centrality classes. Pair ratios \hat{r} were binned linearly on quantity $X(p_t) \equiv 1 - \exp\{-(m_t - m_\pi)/0.4\}$ GeV $\in [0, 1]$ ($m_t = \sqrt{p_t^2 + m_\pi^2}$, pion mass m_π assumed) with bin size 1/25 to achieve nearly uniform statistical accuracy over the binned acceptance. Small-momentum-scale correlations (low- $X(p_t)$ peaks), attributed to quantum correlations (HBT) and Coulomb interactions based on MC simulations [15, 16], were removed by discarding sibling and mixed pairs with $|\eta_1 - \eta_2| < 0.3$, $|\phi_1 - \phi_2| < \pi/6$ (azimuth), $|p_{t1} - p_{t2}| < 0.15$ GeV/c, if $p_t < 0.8$ GeV/c for either particle.

The dominant features in Fig. 1 are 1) a large-momentum-scale correlation (LSC) ‘saddle’ structure with positive (negative) curvature along the $X(p_t)_{\Sigma(\Delta)} \equiv X(p_{t1}) + (-) X(p_{t2})$ sum (difference) direction and 2) a narrow peak structure at large $X(p_t)$ ($p_t > 0.6$ GeV/c). With increasing centrality the negative curvature of the LSC saddle along the difference variable increases in magnitude, the positive curvature along the sum variable decreases, and the magnitude of the peak at large $X(p_t)$ also decreases. The same analysis applied to Pb-Pb collisions in $1.1 < y_{cm} < 2.6$ at the CERN SPS observed no statistically-significant CI correlations [17].

Per-bin statistical errors for $\hat{r} - 1$ in Fig. 1 are $\sim 15\%$ of the maximum correlation amplitude for each centrality. Systematic errors [4] are dominated by contamination from non-primary background particles, mainly weak-decay daughters [18]. Correlations from the latter were assumed to vary from zero to the same correlation amplitude as primary particles. Multiplicative corrections (not applied to Fig. 1) and total systematic errors for $\hat{r} - 1$ were obtained from the average and half difference of the limiting cases and varied from 1.07 and $\pm 7\%$ for $X(p_{t1,2}) > 0.4$ up to 1.16 and $\pm 16\%$ for $X(p_{t1,2}) < 0.4$ and 1.12 and $\pm 12\%$ in the off-diagonal corners. Resonance decays (ρ^0, ω) were estimated [16] to contribute a small saddle-shape correlation with amplitude $\sim 0.0002(\bar{N}_{\text{most-central}}/\bar{N})$ at the corners of each panel of Fig. 1, with curvature opposite to data.

The features of Fig. 1 can be described by two physically-motivated models, the first (saddle) describing local temperature and/or collective velocity fluctuations on (η, ϕ) , the second (large- $X(p_t)$ peak) representing semi-hard scattering correlations and determined from p-p collisions at RHIC [19]. An equilibrated system is described by global temperature parameter $\beta_0 \equiv 1/T_0$. If the system is partially equilibrated the local velocity/temperature distribution can be represented by event-wise changing distribution $\beta(\eta, \phi)$, determining the shapes of the effective *local-parent* p_t spectra $\exp\{-\beta(\eta, \phi)(m_t - m_\pi)\}$ sampled event-wise by final-

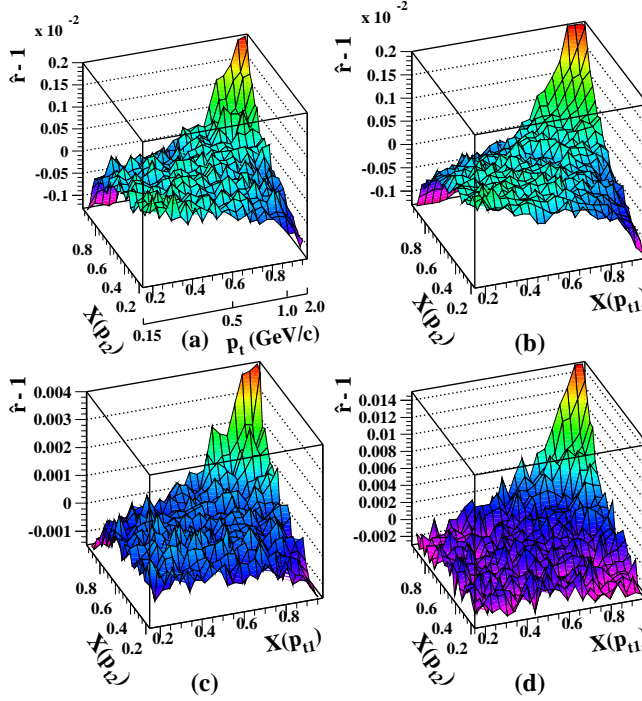


FIG. 1: Symmetrized pair-density net ratios $\hat{r}[X(p_{t1}), X(p_{t2})] - 1$ for all nonidentified charged primary particles for (a) most-central, (b) mid-central, (c) mid-peripheral, and (d) peripheral Au-Au collision events. Note scale change for panels (c) and (d) and auxiliary p_t scale in units GeV/c .

state hadrons. Fluctuations in β linearly represent fluctuations in $1/T$ and/or v/c of the local-parent p_t spectra. If the distribution of β values over an event ensemble is represented by $g_1(\beta)$, with centroid β_0 and variance σ_β^2 , the p_t spectrum is given by convoluting thermal spectrum $e^{-\beta(m_t - m_\pi)}$ with $g_1(\beta)$. If $g_1(\beta)$ is modeled by a gamma distribution [20] then $1/p_t dN/dp_t = A/\{1 + \beta_0(m_t - m_\pi)/n\}^n$, a Lévy distribution [21]. Exponent $1/n \equiv \sigma_\beta^2/\beta_0^2$ is the *relative variance* of $g_1(\beta)$.

By a similar argument hadron pairs sample local-parent two-particle p_t spectra with shapes determined by two-dimensional (2D) temperature/velocity distribution $g_2(\beta_1, \beta_2)$. For uncorrelated β fluctuations or mixed pairs (particles from different events) g_2 factorizes, $g_2(\beta_1, \beta_2) = g_1(\beta_1) \cdot g_1(\beta_2)$, implying zero covariance. For *global* fluctuations (event-wise-uniform β) $g_2(\beta_1, \beta_2) \propto g'_1(\beta_1)\delta(\beta_1 - \beta_2)$: a diagonal locus with maximum covariance. The inclusive two-particle (p_{t1}, p_{t2}) spectrum is the convolution of thermal spectrum $e^{-\beta_1(m_{t1} - m_\pi)}e^{-\beta_2(m_{t2} - m_\pi)}$ with $g_2(\beta_1, \beta_2)$. If $g_2(\beta_1, \beta_2)$ is modelled by a 2D gamma distribution with arbitrary covariance, the two-particle (p_{t1}, p_{t2}) spectrum is well approximated by 2D Lévy model distribution

$$F_{sib} \propto \left(1 + \frac{\beta_0 m_{t\Sigma}}{2n_\Sigma}\right)^{-2n_\Sigma} \left[1 - \left(\frac{\beta_0 m_{t\Delta}}{2n_\Delta + \beta_0 m_{t\Sigma}}\right)^2\right]^{-n_\Delta} \quad (2)$$

on sum and difference variables $m_{t\Sigma} \equiv m_{t1} + m_{t2} - 2m_\pi$ and $m_{t\Delta} \equiv m_{t1} - m_{t2}$. $1/n_\Sigma$ and $1/n_\Delta$ are relative variances of $g_2(\beta_1, \beta_2)$ along sum and difference variables β_Σ and β_Δ respectively, and $\Delta(1/n)_{tot} \equiv 1/n_\Sigma - 1/n_\Delta$ is the relative *covariance* [22] measuring velocity/temperature correlations. Mixed-pair distribution $F_{mix}(p_{t1}, p_{t2})$, a product of single-particle Lévy distributions, has the form of Eq. (2) but with $n_\Sigma = n_\Delta = n$ (g_2 has zero covariance). Ratio $r_{model} \equiv F_{sib}/F_{mix}$ was used to fit data in Fig. 1. Relative variance differences $\Delta(1/n)_\Sigma \equiv (1/n_\Sigma - 1/n)$ and $\Delta(1/n)_\Delta \equiv (1/n_\Delta - 1/n)$ measure *curvatures* of \hat{r} along sum and difference axes at the origin.

Data in Fig. 1 (excluding peak region $X(p_t)_\Sigma > 1.6$) were fitted with $r_{model} - 1 + \mathcal{C}$ by varying parameters n_Σ , n_Δ and \mathcal{C} (offset). Parameter $\beta_0 = 5 \text{ GeV}^{-1}$ is fixed by the inclusive p_t distribution for $p_t < 1 \text{ GeV}/c$. Parameter $1/n \equiv 1/n_{flow} + 1/n_{fluct}$, also obtained from the p_t distribution, represents a combination of transverse expansion (radial flow) and velocity/temperature fluctuations (including hard scattering). Since component $1/n_{fluct}$ relevant to the Lévy saddle fit is not accessible, fits to 2D $\hat{r} - 1$ distributions weakly constrain absolute quantities $1/n_\Sigma$ and $1/n_\Delta$. However, differences $\Delta(1/n)_\Sigma, \Delta(1/n)_\Delta$ are well determined by the saddle curvatures nearly independently of $1/n_{fluct}$. A value $1/n_{fluct} = 0.03$ near the center of the allowed range $1/13$ [18] to 0.0012 (Table I) provided stable $\Delta(1/n)_\Sigma$ and $\Delta(1/n)_\Delta$ fit values. Best-fit parameters and χ^2/DoF for the saddle fits are listed in Table I. The model function and residuals for the fit to centrality (b) are shown in Fig. 2.

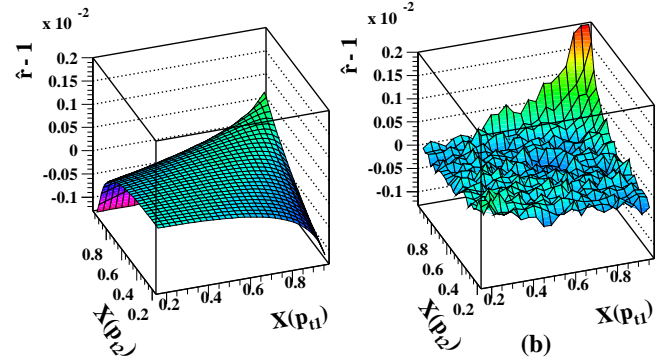


FIG. 2: Left: pair-density net ratio $r_{model}[X(p_{t1}), X(p_{t2})] - 1$ for model fit to mid-central (b) Au-Au collisions. Right: residuals (data - model) for mid-central collisions.

Two-dimensional saddle-fit residuals, as in Fig. 2, are independent of difference $X(p_t)_\Delta = X(p_{t1}) - X(p_{t2})$: the Lévy temperature fluctuation model adequately describes the saddle structure. Residuals from the fit for mid-central events (b) are shown in Fig. 3 (left panel) projected onto sum variable $X(p_t)_\Sigma$. Residuals for other centralities are similar, but differ in amplitude. We speculate that this residual structure is due to semi-hard parton scattering (minijets) [19]. Centrality dependence on mean participant path length ν [23] of efficiency-corrected *per-particle* model parameters $\mathcal{S}\bar{N}\Delta(1/n)$ [24]

which determine saddle amplitudes in Fig. 1 are shown in Fig. 3 (right panel). Linear trends are notable.

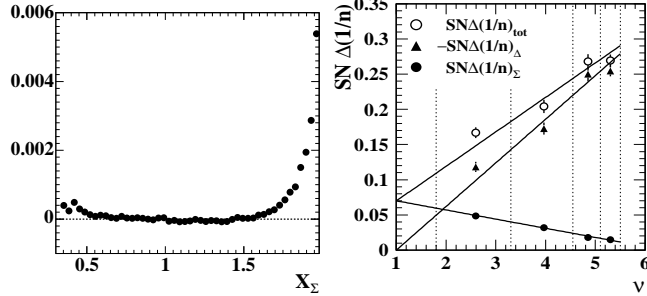


FIG. 3: Left: Residuals from 2D Lévy saddle fit to mid-central (b) data in Fig. 1 projected onto sum variable $X(p_t)_\Sigma$. Right: Efficiency-corrected *per-particle* saddle-curvature measures [24] on centrality ν : $S\bar{N}\Delta(1/n)_\Sigma$ (dots), $-S\bar{N}\Delta(1/n)_\Delta$ (triangles) and $S\bar{N}\Delta(1/n)_{tot}$ (open circles). Linear trends on mean participant path length ν [23] are notable. Data symbols include fitting errors only [25].

If σ_β^2 were dominated by temperature fluctuations ($\beta \rightarrow 1/T$), this fixed-scale (full-acceptance) correlation measurement of saddle curvatures would set a *lower* limit on local temperature fluctuations (or *upper* limit on global fluctuations) $\sigma_\beta/\beta_0 \rightarrow \sigma_T/T_0 \geq \sqrt{\Delta(1/n)_{tot}/2} \sim 1\%$ for central events. The upper limit $\sigma_T/T_0 \leq \sqrt{1/n} \sim 30\%$ on local fluctuations is derived from the inclusive p_t distribution. Local β fluctuations are studied in more detail *via* direct measurement of p_t correlations on (η, ϕ) . We further interpret the correlation structure in Fig. 1 in terms of in-medium modification of a two-particle fragmentation function on (p_{t1}, p_{t2}) . Minijet production in A-A collisions should increase linearly with mean path

length ν [23]. That expectation is consistent with observed linear increase of total curvature $S\bar{N}\Delta(1/n)_{tot}$ in Fig. 3. We also observe in Fig. 3 a) reduced curvature along the sum direction and b) increased curvature along the difference direction which may represent respectively transport of semi-hard parton structure to lower p_t and a more correlated bulk medium. Given the minijet interpretation of $S\bar{N}\Delta(1/n)_{tot}$, combined trends a) and b) represent strong evidence for increased parton dissipation in the more central Au-Au collisions and may be compared to the observed suppression of R_{AA} in central Au-Au collisions at RHIC [27].

HJING [7], which models color-string fragmentation and minijets, exhibits excessive correlation structure at low and high p_t ($X(p_t)_\Sigma < 0.5$ and > 1.6 , respectively) compared to data and a saddle shape which is qualitatively different from the 2D Lévy model and data. RQMD [8], a resonance-gas model, predicts a saddle-shape as well, but with amplitude and form also qualitatively different from Lévy model and data. Fit *residuals* for HJING and RQMD are much more structured and with much larger amplitudes than the data saddle fits themselves.

In conclusion, the dynamical origins of excess $\langle p_t \rangle$ fluctuations [4, 5] in Au-Au collisions at RHIC are probed in this first analysis of two-particle correlations on (p_{t1}, p_{t2}) . The velocity/temperature structure of heavy ion collisions implied by these correlations is unanticipated by theoretical models. The observed correlations on (p_{t1}, p_{t2}) may be interpreted as resulting from semi-hard parton scattering and subsequent fragmentation in which partons are strongly modified by in-medium dissipation in the more central Au-Au collisions. In this picture, with increasing centrality the two-particle fragmentation function is shifted to lower p_t , asymptotically approaching a form consistent with a structured velocity/temperature distribution (Lévy saddle) as an aspect of incomplete equilibration. These newly-observed p_t correlations may thus reveal dissipative modification of the two-particle parton fragmentation function in the medium produced by Au-Au collisions at RHIC.

We thank the RHIC Operations Group and RCF at BNL, and the NERSC Center at LBNL for their support. This work was supported in part by the HENP Divisions of the Office of Science of the U.S. DOE; the U.S. NSF; the BMBF of Germany; IN2P3, RA, RPL, and EMN of France; EPSRC of the United Kingdom; FAPESP of Brazil; the Russian Ministry of Science and Technology; the Ministry of Education and the NNSFC of China; Grant Agency of the Czech Republic, FOM and UU of the Netherlands, DAE, DST, and CSIR of the Government of India; Swiss NSF; and the Polish State Committee for Scientific Research.

TABLE I: Parameters and fitting errors (only) for 2D velocity/temperature fluctuation model for each centrality bin, (a) - (d) (central - peripheral as in Fig. 1). Errors (last column) represent fitting uncertainties. Systematic errors are 7-12% [25]. Extrapolation factors \mathcal{S} are listed in the last row [26].

centrality	(d)	(c)	(b)	(a)	error ^a (%)
\bar{N}	115.5	424.9	790.2	983.0	
$C \times 10^4$	-11.6	-0.820	0.787	0.750	6-14
$\Delta(1/n)_\Sigma \times 10^4$	3.54	0.611	0.183	0.118	6-24
$\Delta(1/n)_\Delta \times 10^4$	-8.61	-3.33	-2.53	-2.04	6-3
$\Delta(1/n)_{tot} \times 10^4$	12.2	3.95	2.71	2.16	
χ^2/DoF	348 286	313 286	475 286	402 286	
\mathcal{S}	1.19	1.22	1.25	1.27	8 ^b

^aRange of fitting errors in percent from peripheral to central.

^bSystematic error.

[1] R. Stock, Nucl. Phys. **A661**, 282 (1999); H. Heiselberg, Phys. Rep. **351**, 161 (2001).

[2] M. Stephanov, K. Rajagopal, E. Shuryak, Phys. Rev. D **60**, 114028 (1999).

- [3] A. Dumitru, R. Pisarski, Phys. Lett. **B504**, 282 (2001).
- [4] J. Adams *et al.* (STAR Collaboration), nucl-ex/0308033.
- [5] S. S. Adler *et al.* (PHENIX Collaboration), nucl-ex/0310005.
- [6] H. Appelshäuser *et al.* (NA49 Collaboration), Phys. Lett. **B459**, 679 (1999); D. Adamová *et al.*, (CERES Collaboration), Nucl. Phys. **A727**, 97 (2003).
- [7] X.N. Wang, M. Gyulassy, Phys. Rev. D **44**, 3501 (1991).
- [8] H. Sorge, H. Stöcker, W. Greiner, Nucl. Phys. **A498**, 567c (1989); Ann. Phys. (N.Y.) **192**, 266 (1989).
- [9] M. Gaździcki, A. Leonidov, G. Roland, Eur. Phys. J. **C6**, 365 (1999).
- [10] T. A. Trainor, eprint hep-ph/0001148, unpublished.
- [11] K. H. Ackermann *et al.*, Nucl. Instrum. Meth. A **499**, 624 (2003); see other STAR papers in volume **A499**.
- [12] Centrality classes d) - a) respectively were defined by N/N_0 cuts at $> 0.029, 0.21, 0.56$ and > 0.79 , corresponding to fraction of total cross section bounds: $> 0.7, 0.4, 0.17$ and > 0.05 . N_0 , the half-maximum point at the end of the minimum-bias distribution plotted as $d\sigma/dN^{1/4}$, is an estimator on N for the maximum number of participants; $N_{part}/N_{part,max} \simeq N/N_0$ within 4%.
- [13] Track-pair cuts required ≥ 10 cm mean track separation in the TPC. Crossing tracks with separations at mid-radius < 10 cm (z) and < 30 cm (azimuth) were removed.
- [14] J. G. Reid and T. A. Trainor, Nucl. Instrum. Meth. A **457**, 378-383 (2001).
- [15] C. Adler *et al.* Phys. Rev. Lett. **87**, 082301 (2001).
- [16] R. Ray and R. Longacre, nucl-ex/0008009, unpublished.
- [17] J. G. Reid, Ph. D. thesis, Univ. of Washington, nucl-ex/0302001.
- [18] Related to but not equivalent to the power-law exponent in C. Adler *et al.*, Phys. Rev. Lett. **87**, 112303 (2001); *ibid.* **89**, 202301 (2002).
- [19] R. J. Porter and T. A. Trainor (STAR Collaboration), hep-ph/0406330.
- [20] M.J. Tannenbaum, Phys. Lett. **B498**, 29 (2001).
- [21] G. Wilk and Z. Włodarczyk, Phys. Rev. Lett. **84**, 2770 (2000); similar to ‘power-law’ distribution [18].
- [22] In the context of velocity/temperature fluctuations this quantity measures $\overline{(\beta_1 - \beta_0)(\beta_2 - \beta_0)}/\beta_0^2$, the relative covariance of velocity/temperature fluctuations.
- [23] $\nu \equiv (N_{part}/2)^{1/3} \simeq 5.5(N/N_0)^{1/3}$ for Au (N_{part} is participant number) [12] estimates mean participant path length in number of encountered nucleons.
- [24] Multiplication by $\mathcal{S}\bar{N}$ [26] gives *per-particle* correlation amplitudes, testing A-A collisions as superpositions of independent p-p collisions, in which case the rescaled correlation amplitudes would be independent of centrality.
- [25] Systematic errors for quantities in Fig. 3, due to systematic uncertainty in the data (7-12%) plus uncertainties in background and efficiency corrections (8%), are 11-14%.
- [26] Extrapolation factor \mathcal{S} (last row in Table I) corrects for contamination and tracking inefficiency [4].
- [27] J. Adams *et al.*, Phys. Rev. Lett. **91**, 172302 (2003).